AERODYNAMIC AND BLADE VORTEX INTERACTION NOISE CHARACTERISTICS ANALYSIS OF ELECTRICALLY CONTROLLED ROTOR BASED ON VISCOUS VORTEX PARTICLE METHOD

Taoyong Su, Yang Lu, Jinchao Ma, Shujun Guan

sutaoyong@126.com, njluyang@163.com, mark.ma@seawings.com.cn, 1164322613@qq.com

National Key Laboratory of Rotorcraft Aeromechanics, College of Aerospace Engineering, Nanjing University of Aeronautics and Astronautics, Nanjing, China

Abstract

An electrically controlled rotor (ECR), also called a swashplateless rotor, replaces a swashplate with a trailing edge flap system to implement primary rotor control. To investigate the aerodynamic characteristics of an ECR in blade-vortex interaction (BVI) condition, an analysis model based on the viscous vortex particle method, ECR blade pitch equation and Weissinger-L lifting surface model is established. In this model, the ECR wake flow field vorticity is discretized as multiple vortex particles, and the vorticity-velocity form Navier-Stokes equation is solved to simulate the transport diffusion of the vorticity. The flap motion induced blade pitch movement is obtained by solving the ECR blade pitch movement equation via the Runge-Kutta fourth-order method. On the basis, BVI noise radiation of an ECR is evaluated using the Ffowcs Williams and Hawkings (FW-H) equation. Based on the present prediction model, the aerodynamic and acoustic characteristics of a sample ECR in BVI condition are analyzed. The results show that since the BVI event of the ECR on the advancing side is mainly caused by the interaction between the flap tip vortex and the blade, the blade spanwise range of ECR BVI occurrence on the advancing side is smaller than that of the conventional rotor. In addition, the magnitude of the maximum sound pressure level on the advancing side as well as on the retreating side of the ECR is also different from that of the conventional rotor, which is consistent with the difference in the airloads between the ECR and conventional rotor.

1. INTRODUCTION

Electrically controlled rotor (ECR), also called as swashplateless rotor, applies blade pitch inputs via trailing edge flap system instead of traditional swashplate mechanism [1]. As the swashplate is eliminated, the control system of the ECR can be simplified, which can effectively reduce the empty weight and the parasite drag of the helicopter [2]. In addition to primary control, applying harmonic or non-harmonic motions, the trailing edge flap system could also be used for rotor vibration reduction [3,4], noise alleviation [5-7] and performance enhancement [8,9].

The helicopter is the quietest Vertical Take-Off and Landing (VTOL) aircraft, but its noise level can still be high enough to compromise its utility unless specific attention is given to designing for low noise [10]. Rotor noise is one of the main sources of helicopter noise, and is usually divided into the deterministic components of thickness noise, loading noise, blade-vortex interaction (BVI) noise, high-speed impulsive (HSI) noise and broadband noise. Among them, BVI noise is essentially a specific type of loading noise, which has an impulsive nature. When a rotor operates in the descent or maneuvering flight, the strong tip vortex released by a blade will approach or even pass through the rotor disc plane and interact with the following blade, resulting in a strong BVI event. This BVI event will lead to impulsive changes in blade airloads, which will not only increase the vibration level of the rotor but also generates BVI noise. Once BVI noise appears, it will extremely annoy people and significantly increase the overall noise level of the helicopter. Therefore, alleviating the BVI noise is always the research focus in the field of helicopter aeroacoustics. With the trailing edge flap system, ECR can theoretically alleviate BVI noise by using active control technology. However, so far researches on ECR have mainly focused on feasibility analysis [11], aerodynamic modeling [1, 12-14], design parameter analysis [15] and performance enhancement [16]. There is no relevant research on the BVI airloads and noise characteristics of an ECR. In fact, because of flap motion, the ECR wake flow field is more complex

Presented at 45th European Rotorcraft Forum, Warsaw, Poland, 17-20 September, 2019

than that of a conventional rotor, which subsequently affects the distributions of the induced inflow and airloads. Improving the basic understanding of BVI phenomenon of ECR is helpful to alleviate the BVI noise by using active blade control techniques.

In the last several decades, considerable efforts have been focused on experiments and numerical prediction of conventional rotor BVI-induced airloads and noise [17-19]. On this foundation, the best-known HART II test campaign was conducted at the DNW low-speed wind tunnel in 2001 by a joint cooperation between DLR, Onera, DNW, US Army AFDD and NASA Langley, which provide experimental insight into the aeroelastic and noise characteristics of a conventional rotor in BVI condition [20-22]. The effects of the higher harmonic pitch control (HHC) inputs on the rotor vibration and BVI noise were also investigated in the experiment. Based on the experimental database, which includes blade elastic deformation, sectional airloads, wake geometry, tip vortex strength, and acoustic radiation measurements, a series of analytical models for the prediction of rotor BVI-induced airloads and noise have been assessed. Incorporating the free wake model into the nonlinear flexible multibody dynamics analysis code, Park compared the predicted results with the HART II experimental data [23]. Gennaretti predicted the BVI-induced airloads and noise using the panel/full-span free wake coupled method [24]. Compared with the free wake model, the full-span free wake model can capture the BVI event more accurately on the advancing and retreating sides. Besides, the full-span free wake model can also improve the prediction of tip vortices trajectories. However, in the research, the vortex core size still needs to be determined preliminarily. With the development of CFD techniques, many researchers have used CFD method to investigate the aerodynamic and acoustic characteristics of helicopter rotor BVI. Reference [25] and [26] show encouraging results in comparison with experimental data for their prediction of BVI-induced airloads from the HART II test. Furthermore, an assessment of the state-of-the-art of CFD-CSD approach for predicting BVI event is provided in reference [27]. Although CFD method has unique advantages in solving rotor blade airloads, the inherent numerical dissipation of most CFD requires very high grid densities to maintain the fidelity of the wake, particularly if the structure of the wake is to be resolved to a level where the high frequency character of the BVI induced airloads can be captured. Therefore, in recent years, researchers have adopted some alternative methods to investigate the BVI phenomenon. Kelly conducted a comprehensive investigation on the application of vorticity transport model (VTM) to the rotor BVI-induced airloads and noise analysis [28,29]. The effects of lifting line model and lifting chord model on the high-frequency sectional airloads as well as the acoustic are also explored. The numerical results show that the VTM is capable of capturing the tip vortices and their roll-up process. Based on the OLS experimental data, Zhao investigated the ability of hybrid method to predict rotor BVI-induced airloads and noise [30]. In addition, the Lattice-Boltzmann Method (LBM) was adopted in Ref. [31] to establish the analytical model. Based on the experimental database from HART II test, the investigation of the rigid blade model and elastic blade model effects on the predicted airloads are also performed.

Accurate prediction of the strength and position of the tip vortices is essential to capture the high frequency oscillating blade airloads induced by BVI. In recent years, viscous vortex particle method (VVPM) has been widely employed in helicopter aerodynamic analysis [32-37]. This method does not rely on empirical parameters and can take the wake viscous effect into account. In addition, since the vorticity-velocity form of incompressible Navier-Stokes equations are solved directly in the Lagrangian frame, the VVPM can avoid the numerical dissipation problem and is an ideal method for accurately predicting the wake vorticity structure in BVI condition. In this paper, based on the VVPM, ECR blade pitch movement equation and Weissinger-L lifting surface model, a BVI-induced airloads prediction model for ECR is established. BVI noise radiation of the ECR is evaluated using a postprocessor for the blade air-loads that implements the Farassat's formulation 1A [38] of the Ffowcs Williams and Hawkings (FW-H) equation [39].

This paper consists of the following sections. In section 2, first, the ECR blade pitch movement equation is provided. Next, the BVI-induced airloads prediction model of ECR established from the VVPM and Weissinger-L lifting surface is elaborated, and the Farassat 1A integral formulation for noise radiation is described. As there is no literature regarding the BVI phenomenon of ECR, in section 3, first, the HART II experimental rotor is used as an example to validate the aerodynamics and acoustics predicted model established in this paper. On this basis, the BVI characteristic of ECR is investigated. Finally, conclusions are outlined in section 4.

Presented at 45th European Rotorcraft Forum, Warsaw, Poland, 17-20 September, 2019

2. ECR BVI-INDUCED AIRLOADS AND NOISE PREDICTION MODEL

2.1. ECR Blade Pitch Movement Equation

ECR achieves blade pitch movement via pitch moment generated by flap deflection, and the blade root usually has very low torsional stiffness. Based on the rigid blade model, the pitch movement equation of the ECR is established and the torsional stiffness of the blade is determined only by the spring at the blade root. Assuming that the gravity center, the aerodynamic center and the elastic center of the blade are located at the $1/4$ chord length, the pitch movement of the blade can be expressed as follows:

(1) $$I_f\ddot{\theta}_f + I_f\Omega^2\left(\theta_{pre} + \theta_f\right) + k_\theta\theta_f = M_\theta$$

In the equation, θ_f is the flap deflection and tennis racket moment induced blade pitch angle; I_f is the blade rotational inertia around the pitch axis; k_θ is the blade root torsion stiffness coefficient; Ω is the rotor rotating speed; θ_{pre} is the blade pre-index angle; M_θ is the flap deflection-induced aerodynamics pitch moment. The flap deflection induced airfoil pitch moment coefficient is calculated via the Hariharan-Leishman unsteady flap aerodynamics model [40] and the blade pitch movement equation is solved via the Runge-Kutta fourth-order method.

2.2. Viscous Vortex Particle Wake Model

The velocity-vorticity form of incompressible Navier-Stokes equation in Lagirange frame can be used to represent the rotor wake vortex flow with a high Reynolds number. In VVPM, the continuous vorticity field is discretized by using vortex particles with certain vorticity. Thus, the governing equation can be expressed in the form of convection-diffusion of N vortex particles:

(2) $$\frac{Dx_i}{Dt} = u\left(x_i, t\right)$$

(3) $$\frac{D\alpha_i}{Dt} = \alpha_i \times \nabla u\left(x_i, t\right) + \nu\nabla^2\alpha_i + S$$

where α_i and x_i are a vortex particle vorticity vector and a position vector respectively, $\mathbf{u}$ is local velocity vector, ν is the kinematic viscosity, $\frac{D}{Dt}$ is the substance derivative, and S is the local vorticity source.

In formula (3), the first term on the right is the stretching-effect term, which represents the effect of stretching and rotation on local vorticity, the second term is the viscous diffusion term, which reflects the viscosity induced vorticity diffusion effect, and the third term is the source term, which indicates that new vortex particles are constantly generated on the blade surface and shed into the rotor wake. The velocity gradient in the stretching term includes the rotor wake vortex particle and rotor blade induced velocity gradient. The vortex particle induced velocity gradient is solved directly:

(4) $$\alpha_i \times \nabla u_{ip} = \left[\sum_{j=1}^{N}\frac{1}{\sigma_{ij}^3}\left[\tilde{\alpha}_j\right]\left[\nabla\left(K(\rho)\left(x_i - x_j\right)\right)\right]\right] ?\, \alpha_i$$

where $\left[\tilde{\alpha}_j\right]$ is an antisymmetric tensor composed of the vorticity vector of a vortex particle, σ_{ij} is the symmetric smoothing parameter and $K(\rho)$ is the Biot-Savart kernel function after the smoothing correction.

The viscous diffusion is determined via a particle strength exchange (PSE) method:

(5) $$\nu\nabla^2\alpha_i = \frac{2\nu}{\sigma_{ij}^2}\sum_{j=1}^{N}\left(V_i\alpha_j - V_j\alpha_i\right)\xi_{\sigma_{ij}}\left(x_i - x_j\right)$$

where V is the volume of a vortex particle, and $\xi_\sigma\left(x - x_i\right)$ is the vortex particle vorticity distribution function after a smoothing correction. The expression of the source term will be provided in the next section.

2.3. Weissinger-L ECR Blade Lifting Surface Model

The rotor wake flow field vorticity convection and diffusion process are simulated via the VVPM, and the specific form of the source term depends on the blade aerodynamic model. In this paper, the Weissinger-L lifting surface model is employed to solve the variation in the ECR blade bound vortex circulation along the span direction, which in turn acquires the source term.

Figure 1 shows the solution diagram of the ECR blade bound vortex lattice and new vortex particle. The trailed vortices and shed vortices are generated due to the bound circulation of blade segments varies spanwise and azimuthally, respectively. When calculating the blade bound vortex circulation distribution at the current azimuth, the near wake is still discretized via the vortex lattice and its circulation is equal to the bound circulation of the blade segment corresponding to the previous azimuth. The position of the vortex lattice trailing edge is determined by the local flow velocity.

Presented at 45th European Rotorcraft Forum, Warsaw, Poland, 17-20 September, 2019

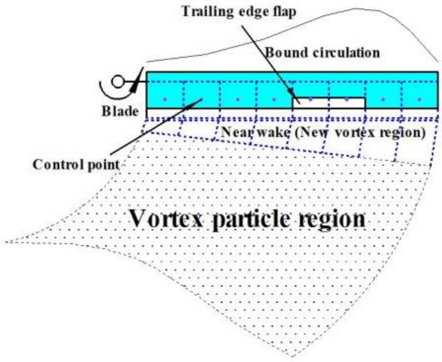

Figure 1. Solution diagram of the vortex lattice bound to the ECR blade surface and new vortex particle.

To solve the blade bound vortex circulation at each segment, a control point is deployed at the $3/4$ blade chord in each vortex lattice. Based on an impenetrable boundary condition, the relation between the bound vortex circulation and locally induced velocity can be represented as follows:

(6) $$\mathbf{A\Gamma_b n = Bn}$$

where $\mathbf{A}$ is the impact coefficient matrix of the bound vortex lattice on the control point, $\mathbf{\Gamma_b}$ is the bound vortex circulation matrix, $\mathbf{B}$ is the impact coefficient matrix of the near wake vortex lattice, wake vortex particle, and blade movement on the blade control point, and $\mathbf{n}$ is the unit normal vector of the blade surface on the control point.

The unit normal vector of the blade surface on the control point is determined by the geometric incidence of the blade segment. Because the trailing edge flap is introduced, the effect of flap deflection and flap overhang on the unit normal vector of the surface can be represented by using the equivalent blade angle of incidence [16]:

(7) $$\alpha_{eff} = \alpha + \frac{1}{\pi}\left(T_{10} - lT_{21}\right)\delta$$

where α_{eff} is the equivalent incidence of the flap segment airfoil for the ECR blade, α is the geometric incidence of the flap segment basic airfoil, δ is the flap deflection angle and downward deflection is positive, l is the non-dimensional flap overhang corresponding to the semi-chord length of the airfoil, T_{10} and T_{21} are constants related to the flap chordwise location. For detailed expressions, please refer to reference [41].

After the blade bound vortex distribution is obtained, the near wake vortex lattice of each blade segment at the current azimuth is replaced by an equivalent vortex particle. The source term in formula (3) can be written as

(8) $$S = -\frac{d\boldsymbol{\omega}_b}{dt} + \mathbf{u}_b \nabla \times \boldsymbol{\omega}_b$$

where $\boldsymbol{\omega}_b$ is the bound vorticity of the blade segment, $\mathbf{u}_b$ is the velocity of the blade segment to the fluid.

Once the iterations of rotor wake and bound circulation converge, the unsteady airloads of the airfoil and the incremental airloads caused by trailing edge flap motion are obtained by using Leishman-Beddoes model [42] and Harihanran-Leishman model [40], respectively.

2.4. BVI Noise Prediction

The evaluation of ECR aerodynamic noise is based on the FW-H equations derived from Lighthill's acoustic analogy approach, which contains monopole sources noise (thickness noise), dipole sources noise (loading noise) and quadrupole sources noise. Due to the BVI event usually occurs in low-speed descent flight, the contribution of the quadrupole noise to the whole acoustic field is very small, so the Farassat's formulation 1A obtained by ignoring the quadrupole noise term in the FW-H equation is used in the noise prediction in this paper. The acoustic pressure $p'(x,t)$ at an observation point can be written as

(8) $$p'(x,t) = p_t'(x,t) + p_l'(x,t)$$

where $p_t'(x,t)$ and $p_l'(x,t)$ are the thickness noise and the loading noise, respectively.

It should be pointed out that the rotor BVI noise is essentially a loading noise. In the case of BVI occurrence, the thickness noise tends to be negligible and the acoustic pressure is dominated by the loading noise.

3. RESULTS AND ANALYSIS

3.1. Validation of the BVI airloads and noise computational model

Currently, there are few ECR related tests, and there is no literature regarding BVI-induced airloads and noise of ECR. Therefore, in this section, the HART II test BL case is used as an example to validate the present BVI-induced airloads and noise predicted model by comparing the blade airloads and the noise footprint on a horizontal plane below the rotor hub. It should be noted that the rotor was trimmed to the experimental thrust coefficient and to zero rolling and pitching moments about the rotor hub in the present simulation, whereas the rolling and pitching moments are 20Nm and -20Nm respectively in the HART II test. In addition, the fuselage effect is not considered in this simulation.

The comparison of the predicted and experimental section normal force C_nM^2 at the 87% span location is given in Figure 2. As shown,

Presented at 45th European Rotorcraft Forum, Warsaw, Poland, 17-20 September, 2019

the predicted airloads fluctuates dramatically around 50° azimuth angle on the advancing side and around 300° on the retreating side, which compares well with the experimental data. However, since the elastic deformation of the blade is not considered in the present analytical model, there are some discrepancies between the predicted airloads and the experimental data. However, there are about some discrepancies between the predicted and measured impulsive airloads phase, because the influence of the fuselage on the induced velocity is not considered.

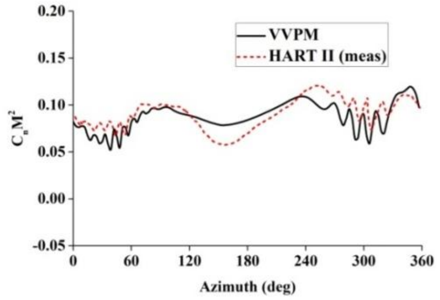

Figure 2. Normal force (C_nM^2) predictions at 87% radial station.

A comparison between the predicted and measured BVI noise footprint on a horizontal plane which placed 1.1075R below the rotor hub is shown in Figure 3. The noise level is filtered to include the frequencies only from the 6th to the 40th blade passage frequency (BPF), which are mainly associated with the BVI event. The simulation results show that two distinct radiation lobes appear in the advancing and retreating sides, which is the same with the experimental data obtained from the HART II test. The location and magnitude of the SPL maximum on the retreating side is an agreement with the measurements very well, while the magnitude of the SPL maximum on the advancing side is slightly underestimated by 2-3 dB, and the location of the SPL maximum on the advancing side is further to the rear of the rotor. In addition, the predicted BVI noise in the center and to the rear of the rotor disc is larger than the measured data because the effect of the fuselage on the absorption and scattering of noise is not considered in the simulation.

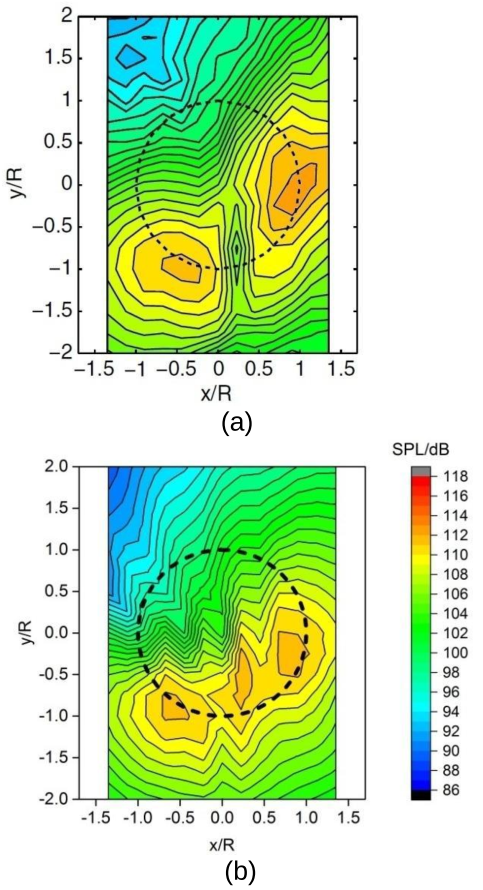

Figure 3. Predicted and measured SPL noise contours (6th-40th BPF). (a) Measured; (b) Predicted.

In the preceding context, the prediction model of BVI airloads and noise has been validated with the HART II test database. The compared results show that the present model is capable of predicting the rotor BVI-induced airloads and noise.

3.2. Analysis of BVI airloads and noise characteristics of ECR

In this section, the HART II test rotor is used as a reference to rebuilding an ECR, and the analysis of the BVI-induced airloads and noise of ECR is also performed under the HART II test BL condition. The main parameters of the sample ECR are listed in Table 1. Other parameters of the ECR are identical to those of the HART II test rotor.

Table 1. The main parameters of a sample ECR.

Pre-index angle	6°
Blade root torsional stiffness	95Nm/rad
Flap chord	0.03025m
Flap spanwise length	0.4m
Flap midspan location	1.4m
Nondimensional flap overhang	0.125

Presented at 45th European Rotorcraft Forum, Warsaw, Poland, 17-20 September, 2019

The deflection of the flaps changes the load distribution along the blade span, which leads to the difference between the wake vorticity distribution of the ECR and that of the conventional rotor. Figure 4 shows the vorticity isosurfaces diagrams of the ECR wake and the conventional rotor wake under the HART II test BL condition. To further illustrate the direction of the vorticity, the vorticity isosurfaces diagram is colored by the vorticity value in the x-direction. Because of the small blade pitch angle, there are no strong tip vortices between the 90° to the 180° azimuth angle on the ECR advancing side. In fact, the predicted result illustrates the strong vortex is shed from the tip of the flap in the second quadrant because of the large flap deflection. Meanwhile, the wake vorticity structure on the retreating side is almost the same as that of the conventional rotor. In addition, both the ECR wake vortices and the conventional rotor wake vortices will rapidly roll up along the rotor advancing and retreating sides.

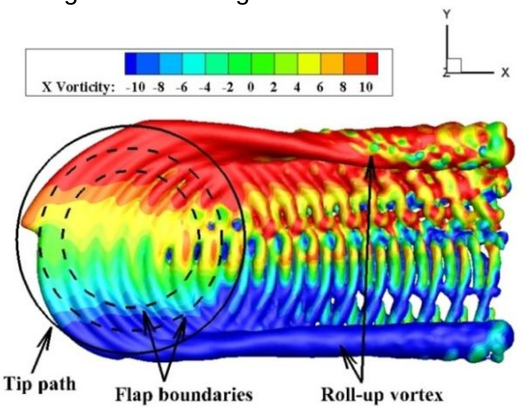

(a)

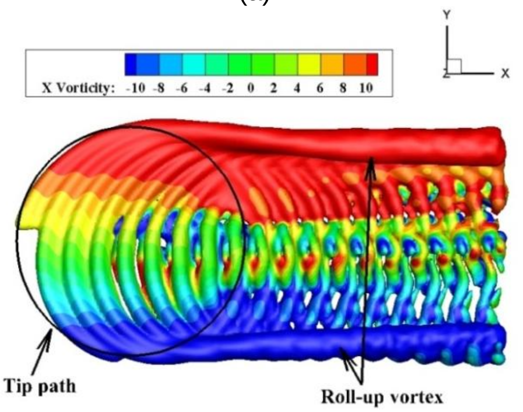

(b)

Figure 4. Vorticity isosurfaces diagram of the wake flow field for ECR and conventional rotor. (a) ECR with 6° pre-index angle; (b) Conventional rotor.

Because of the difference between the ECR and conventional rotor wake structure on the advancing side, when the BVI occurs, the amplitude and location of the impulsive airloads of the ECR on the advancing side will be quite different from those of the conventional rotor. Figure 5 (a) and Figure 5 (b) show the section normal force distribution of the ECR and conventional rotor, respectively. Although due to the flap motion, the section normal force distribution of the ECR is quite different from that of the conventional rotor, both the ECR and conventional rotor BVI-induced impulsive airloads on the advancing and retreating side can be observed. Furthermore, the spanwise range of the ECR BVI occurrence on the advancing side is smaller than that of the conventional rotor, especially around the 50° azimuth angle. As mentioned above, the BVI event of the ECR on the advancing side is mainly caused by the interaction between the flap tip vortices and the blades. The theoretical interaction region of ECR and conventional rotor on the advancing side are also shown in Figure 5 (a) and Figure 5 (b), respectively. The difference in the theoretical interaction region between the ECR and the conventional rotor is the main reason for the different width of the BVI occurrence. On the retreating side, the amplitude of the ECR impulsive airloads is slightly less than those of the conventional rotor.

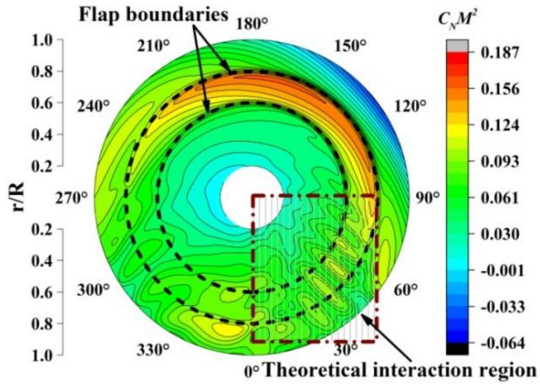

(a)

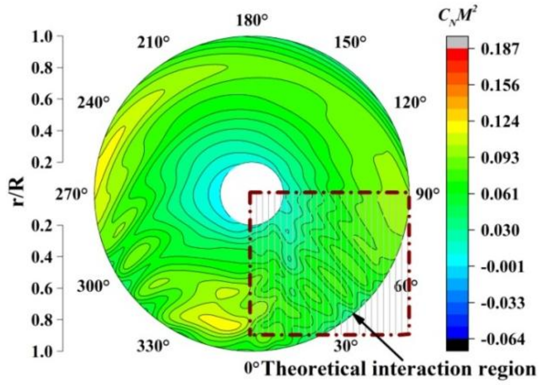

(b)

Figure 5. BVI-induced airloads of ECR and conventional rotor. (a) Disc airloads distribution of the ECR with 6° pre-index angle; (b) Disc airloads distribution of the conventional rotor.

Presented at 45th European Rotorcraft Forum, Warsaw, Poland, 17-20 September, 2019

Based on the predicted BVI-induced airloads of the ECR, the BVI noise footprint of the ECR on a horizontal plane which placed 1.1075R below the rotor hub is given in Figure 6. The noise levels are still filtered to include only the frequencies between 6-40 times BPF. The magnitude of the SPL maximum on the advancing side of the ECR is 4dB higher than that of the conventional rotor, which is caused by the larger ECR airloads on the advancing side. The magnitude of the SPL maximum on the retreating side and the center of the ECR are 3dB less than that of the conventional rotor, although the amplitude of the BVI-induced airloads on the retreating side of the ECR is just slightly less than that of the conventional rotor.

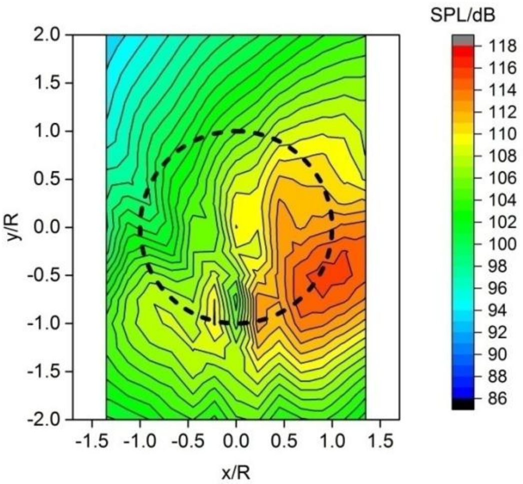

Figure 6. Predicted SPL noise (6th-40th BPF) contours of the ECR with 6° pre-index angle.

4. CONCLUSIONS

In this paper, based on the viscous vortex particle method, ECR blade pitch movement equation and Weissinger-L lifting surface model, a predicted model for ECR BVI-induced airloads is established. In the model, the effects of flap deflection on the blade bound vortex circulation distribution are considered by using the equivalent angle of incidence. The flap deflection induced blade pitch movement is obtained by solving the ECR blade pitch movement equation via the Runge-Kutta fourth-order method. On this basis, BVI noise radiation of an ECR is evaluated using a postprocessor for the blade airloads that implements the Farassat's formulation 1A of the FW-H equation. The predicted model was validated against the well known HART II test database. Furthermore, the aerodynamic and acoustic characteristics of a sample ECR in BVI conditions are analyzed. The following conclusions have been drawn from the present study:

1. The BVI-induced airloads predicted model established in this paper is capable of accurately predicting the wake structure in BVI condition. In addition, the magnitude of the predicted SPL maximum on the retreating side is an agreement with the measurements very well, while the magnitude of the SPL maximum on the advancing side is slightly underestimated.
2. Since the BVI event of the ECR on the advancing side is mainly caused by the interaction between the flap tip vortices and the blades, the blade spanwise range of the ECR BVI occurrence on the advancing side is smaller than that of the conventional rotor. The magnitude of the SPL maximum on the advancing side of the ECR with 6° pre-index angle is higher than that of the conventional rotor, which is consistent with the predicted airloads on the advancing side. The magnitude of the SPL maximum on the retreating side and the center of the ECR are less than that of the conventional rotor.

5. REFERENCES

[1] Su TY, Lu Y. Application of viscous vortex particle method to electrically controlled rotor wake and aerodynamic characteristics analysis. Proceeding of the 7th Asian/Australian Rotorcraft Forum; 2018 Oct. 30-Nov. 1; Jeju Island, Korea.
[2] Shen JW, Chopra I. Swashplateless helicopter rotor with trailing edge flaps. Journal of Aircraft 2004;41(2):208-214.
[3] Viswamurthy SR, Ganguli R. An optimization approach to vibration reduction in helicopter rotors with multiple active trailing edge flaps. Aerospace Science and Technology 2004;8(3):185-194.
[4] Roget B, Chopra I. Wind tunnel testing of rotor with individually controlled trailing edge flaps for vibration reduction. Journal of Aircraft 2008;45(3):868-879.
[5] Patt D, Liu L, Friedmann PP. Simultaneous vibration and noise reduction in rotorcraft using aeroelastic simulation. Journal of the American Helicopter Society 2006;51(2):127-140.
[6] Sim BW, Janakiram RD, Barbely NL, Solis E. Reduced in-plane, low frequency noise of an active flap rotor. Proceedings of the 65th American Helicopter Society Annual Forum; 2009 May 27-29; Grapevine, TX.
[7] Sim BW, Potsdam M, Kitaplioglu C, LeMasurie P, Lorber P, Andrews J. Localized, non-harmonic active flap motions for low frequency in-plane rotor

Presented at 45th European Rotorcraft Forum, Warsaw, Poland, 17-20 September, 2019

noise reduction. Proceedings of the 68th American Helicopter Society Annual Forum; 2012 May 1-3; Fort Worth, TX.
[8] Liu L, Friedmann PP, Kim I, and Bernstein, DS. Rotor performance enhancement and vibration reduction in presence of dynamic stall using actively controlled flaps. Journal of the American Helicopter Society 2008;53(4) : 338-350.
[9] Ravichandran K, Chopra I, Wake BE, Hein B. Trailing edge flaps for rotor performance enhancement and vibration reduction. Journal of the American Helicopter Society 2013;58, 022006.
[10] Johnson W. Rotorcraft aeromechanics. Cambridge University Press, New York, NY, 2013, pp. 493-544.
[11] Ormiston RA. Aeroelastic considerations for rotorcraft primary control with on-blade elevons. Proceedings of the 57th American Helicopter Society Annual Forum; 2001 May 9-11; Washington DC.
[12] Shen JW, Chopra I. Swashplateless helicopter rotor with trailing edge flaps. Journal of Aircraft 2005;41(2):208-214
[13] Shen JW, Chopra I. Aeroelastic modeling of trailing edge flap helicopter rotors including actuator dynamics. Journal of Aircraft 2004;41(6): 1465-1472.
[14] Falls J. Design and performance prediction of swashplateless helicopter rotor with trialing edge flaps and tabs [dissertation]. University of Maryland: 2010.
[15] Shen JW, Chopra I. A parametric design study for a swashplateless helicopter rotor with trailing edge flaps. Journal of the American Helicopter Society 2004; 49(1):43-53.
[16] Lu Y, Wang C. Active control for performance enhancement of electrically controlled rotor. Chinese Journal of Aeronautics 2015;28(5):1494-1502.
[17] Schmitz FH, Yu YH. Helicopter impulsive noise: theoretical and experimental status. Journal of Sound and Vibration 1986;109(3):361-422.
[18] Yu YH, Tung C, Gallman J, Schultz KJ, Wall BG, Spiegel P, and Michea B. Aerodynamics and acoustics of rotor blade-vortex interactions. Journal of Aircraft 1995;32(5):970-977.
[19] Strawn RC, Duque EP, Ahmad J. Rotorcraft aeroacoustics computations with overset-grid CFD methods. Journal of the American Helicopter Society 1999;44(2):132-140.
[20] Wall BG, Burley CL, Yu Y, Richard H, Pengel K, and Beaumier P. The HART II test – measurement of helicopter rotor wakes. Aerospace Science and Technology 2004;8(2004):273-284.
[21] Wall BG. 2nd HHC aeroacoustic rotor test (HART II)-part I: test documentation. Institute Report, IB 111-2003/31, DLR, 2003.
[22] Wall BG, Burley CL. 2nd HHC aeroacoustic rotor test (HART II) – part II: representative results. Institute Report, IB 111-2005, DLR, 2005.
[23] Park JS, Jung SN, Park SH, and Yu YH. Correlation study of a rotor in descending flight using DYMORE with a freewake model. Journal of Mechnical Science and Technology 2010;24(8):1583-1594.
[24] Gennaretti M, Bernardini G, Serafini J, and Romani G. Rotorcraft comprehensive code assessment for blade vortex interaction conditions. Aerospace Science and Technology 2018;80(2018):232-246.
[25] Broy DD. HART II acoustic predictions using a coupled CFD/CSD method. Proceedings of the 65th American Helicopter Society Annual Forum; 2009 May 27-29; Grapevine, Texas.
[26] Lim JW, Strawn RC. Prediction of HART II rotor BVI loading and wake system using CFD/CSD loose coupling. 45th AIAA Aerospace Sciences Meeting and Exhibit; 2007 January 8-1; Reno, Nevada
[27] Smith MJ, Lim JW, Wall BG, Baeder JD, Biedron RT, Boyd DD, Jayaraman B, Jung SN, and Min BY. An assessment of CFD/CSD prediction state of the art using the HART II international workshop data. Proceedings of the 68th American Helicopter Society Annual Forum; 2012 May 1-3; Worth, TX.
[28] Kelly ME, Brown RE. Influence of blade aerodynamic model on prediction of helicopter rotor high-frequency airloads. Journal of Aircraft 2011;48(2):476-494.
[29] Kelly ME, Brown RE. Influence of blade aerodynamic model on prediction of helicopter rotor aeroacoustic signatures Journal of Aircraft 2011;48(3):1058-1083.
[30] Zhao YY, Shi YJ, and Xu GH. Helicopter blade vortex interaction airload and noise prediction using coupling CFD/VVPM method. Applied Sciences 2017;7(381):1-20.
[31] Romani G, Casalino D. Rotorcraft blade vortex interaction noise prediction using the Lattice-Boltzmann method. Aerospace Science and Technology 2019;88(2019):147-157.

Presented at 45th European Rotorcraft Forum, Warsaw, Poland, 17-20 September, 2019

[32] He CJ, Zhao JG. Modeling rotor wake dybamics with viscous vortex particle method. AIAA Journal 2009;47(4):902-915.
[33] Tan JF, Wang HW. Simulating unsteady aerodynamics of helicopter rotor with panel/viscous vortex particle method. Aerospace Science and Technology 2013;30(2013):255-268.
[34] Shi YJ, Xu GH, and Wei P. Rotor wake and flow analysis using a coupled Eulerian-Lagrangian method. Engineering Applications of Computational Fluid Mechanics 2016;10(1):386-404.
[35] Singh P, Friedmann PP. Application of vortex methods to coaxial rotor wake and load calculations in hover. Journal of Aircraft 2018; 55(1):373-381.
[36] Tan JF, Zhou TY, Sun YM, and Barakos GN. Numerical investigation of the aerodynamic interaction between a tiltrotor and a tandem rotor during shipboard operations. Aerospace Science and Technology 2019; 87(2019):62-72.
[37] Lu Y, Su TY, Chen RL, Li P, Wang Y. A method for optimizing the aerodynamic layout of a helicopter that reduces the effects of aerodynamic interaction. Aerospace Science and Technology 2019;88(2019):73-83.
[38] Farrasate F. Derivation of formulations 1 and 1A of Farassat. NASA/TM Report; 2007 Report NO.: TM-2007-214853.
[39] Ffowcs Williams JE, Hawkings DL. Sound generation by turbulence and surfaces in arbitrary motion. Philosophical Transactions of the Royal Society of London. Series A, Mathematical and Physical Sciencs 1969;264(1151):321-342.
[40] Hariharan N, Leishman JG. Unsteady aerodynamics of a flapped airfoil in subsonic flow by indicial concepts. 36th AIAA/ASME/ASCE/AHS/ASC Structures, Structural Dynamics, and Materials Conference; 1995 April 10-12; New Orleans, LA.
[41] Garrick IE. Propulsion of a flapping and oscillating airfoil. NACA TR 567, 1936.
[42] Leishman JG, Beddoes TS. A generalized method for unsteady airfoil behavior and dynamic stall using the indicial method. Proceedings of the 42th American Helicopter Society Annual Forum;1986 June 2-4; Washington D.C..
[43] Bhagwat MJ, Ormistion RA, Saberi HA, and Xin H. Application of CFD/CSD coupling for analysis of rotorcraft airloads and blade loads in maneuvering flight. Proceedings of the 63th American Helicopter Society Annual Forum; 2007 May 1-3; Virginia Beach, VA.

Presented at 45th European Rotorcraft Forum, Warsaw, Poland, 17-20 September, 2019